



ON THE ROLE OF LEADING-EDGE BUMPS IN THE CONTROL OF STALL ON-SET IN AXIAL FAN BLADES

Alessandro CORSINI¹, Giovanni DELIBRA¹, A. Geoff SHEARD²

¹*Sapienza University of Rome, Dept. of Mechanical and Aerospace Engineering, Via Eudossiana 18, 00184 Roma, Italy*

²*Fläkt Woods Limited, Axial Way, Colchester, Essex, CO4 5ZD, UK*

SUMMARY

Biologists have associated the capability of the humpback whale to execute very sharp rolls and loops under water with the presence of bumps on the leading edge of their flukes that work as a stall-control system. Taking a lead from the humpback whale flukes, this paper reports on a three-dimensional numerical study of sinusoidal leading edges on cambered airfoil profiles. The authors computed the turbulent flow around the cambered airfoils at different angles of attack with the open source solver OpenFOAM and an isotropic eddy viscosity model integrated to the wall. The reported research focused on the effects of the modified leading edge in terms of lift-to-drag performance. The research was primarily concerned with the elucidation of the fluid flow mechanisms induced by the bumps and the impact of those mechanisms on airfoil performance.

INTRODUCTION

Aerodynamicists, in academy and industry, continuously struggle to increase blade pressure rise and loading in turbomachinery. However, the operating range of fans and compressors is constrained as the rise of instabilities on the blade surface with the aerodynamic load inevitably results in operational limits (see, for example [1]). Two main types of aerodynamic flow instability exist in compressors: (i) 'rotating stall' (in which regions of reversed flow occur locally); and (ii) 'surge' (which is characterised by periodic backflow over the entire annulus involving violent oscillations in the compression system). The first of these, 'rotating stall', is a mechanism by which the rotor adapts to a reduction in flow rate, which results in circumferentially non-uniform flow patterns rotating in the annulus.

In both compressors and fans, rotating stall is associated with efficiency loss, and noise and vibrations. These aerodynamic flow instabilities place considerable mechanical stress on the rotors, which can eventually lead to mechanical failure. In turbomachinery design and operation, stall control is regarded as a key technology that facilitates the development of high-pressure fans and compressors. Specifically the use of variable pitch motion blades [2], [3] has largely eliminated in-service mechanical failures associated with parallel operation of low-speed fans. Although still in its

infancy when compared to the turbomachinery community, the industrial fan one is now embracing three-dimensional blade design [4].

Although the operating limits of both industrial fan and compressors have been substantially increased through the application of established stall control methodologies, e.g. [5] and [6], the continuing quest for improved aerodynamic performance drives researchers to look for new design solutions. One possible source of inspiration comes from biomimetics, the examination of nature, its models and processes to take inspiration from or to emulate in man-made designs. Evolution has provided *animalia* and *plantae* with millennia to adapt, survive and develop. Today, researchers study nature models and processes, and in so doing gain insight into the physics underpinning them. Within the context of turbomachinery blade design, natural flyers and swimmers provide a wide range of elegant aerodynamic solutions. Some of these solutions are difficult, if not impossible to replicate. Try to imagine the difficulties in building a mechanical bat, replicating its flexible wings, with over 10 different mobile junctions necessary to reproduce its complex flapping [7]. However, despite the difficulty inherent in the approach, the insight it provides is a source of inspiration.

Among the pioneering studies on biology-based concepts for hydrodynamics, Fish [8] analysed the efficiency of swimming mammals highlighting the drag reduction mechanisms that developed with the evolutionary process. The same author in [9] described passive and active flow control mechanisms in natural swimmers and their technological exploitability. Hua *et al.* [10] carried out a biomimetic study on stall. The researchers conducted a numerical investigation to establish the performance of a seagull wing specifically studying the impact of the wing's natural camber. They presented the advantages of a naturally cambering wing by comparing its lift-to-drag ratio against a NACA four digit airfoil.

Despite the promise of nature-inspired solutions to turbomachinery stall control, the researches reported in the literature present concepts that can not be exploited by industrial fan design engineers. The route of evolution in maximising lift and minimising drag occurs over a range of Reynolds numbers that are simply too low for turbomachinery applications.

In contrast with the above reservation with respect to Reynolds number, the humpback whale (*Megapteranovaeangliae*) is one of the few animals that can provide information and inspiration for turbomachinery design. This particular mammal is able to perform sharp rolls and loops under water whilst hunting. Marine biologists attribute this capability to the peculiar shape of its flippers (Figure 1), characterised by a wing-like aspect ratio and a wavy leading edge with typically ten or eleven rounded tubercles. According to Fish and Battle [11], the inter-tubercle distance is constant and the first tubercle is placed at about 30% of the span. Additionally the flippers profile has a cross-section that is constant irrespective of the span-wise position, whilst the chord reduces moving outward. Figure 2 illustrates a sketch of the flipper.



Figure 1: Humpback whale (left); detail of the whale pectoral fin or flipper with its tubercles (right)

Researchers have associated tubercles with the same mechanism that is induced on the flow field by aircraft strakes: the capability to keep the boundary layer attached over the wing and in so doing maintaining lift at higher angles of attack (AoA). The tubercles therefore act as a stall-control system.

Among hydrodynamics studies, van Nierop *et al.* [12] analytically investigated the mechanism which the presence of the tubercle induced on a two-dimensional model. They modelled the tubercles as leading edge bumps and reached two primary conclusions. First, that increasing the amplitude of the bumps flattens the lift curve. Second, that the stall-delay effect was insensitive to the bump distribution's wavelength. Johari *et al.* [13] measured lift, drag and pitching moment on a NACA 63₄-021 profile with a modified sinusoidal leading edge at Reynolds number of 183,000 over a range of $6 \leq \alpha \leq 30$ deg. They investigated the effect at different amplitudes of the sinusoid ranging from 2.5% to 12% of the chord. They observed increased drag and decreased lift for AoA smaller than the corresponding baseline stall AoA. However, at angle larger than the corresponding baseline stall AoA they observed increased lift of about 50% of the corresponding baseline profile's lift. This increase in lift was achieved with almost no increase in drag. The research of Johari *et al.* [13] indicates that the sinusoid's wavelength is not an influential parameter on aerofoil performance. In contrast, the sinusoid's amplitude has a distinct and positive effect on lift performance.

Pedro and Kobayashi [14] performed a numerical stall delay study on the 'real geometry' of humpback whale flippers. They concluded that the improved aerodynamic performance associated with the "wavy" leading edge of the flipper was due to the presence of streamwise vortices originating from the tubercles. This phenomenon was exploited by WhalePower [15] who patented humpback whale tubercled technology and applied it to ceiling fan design.

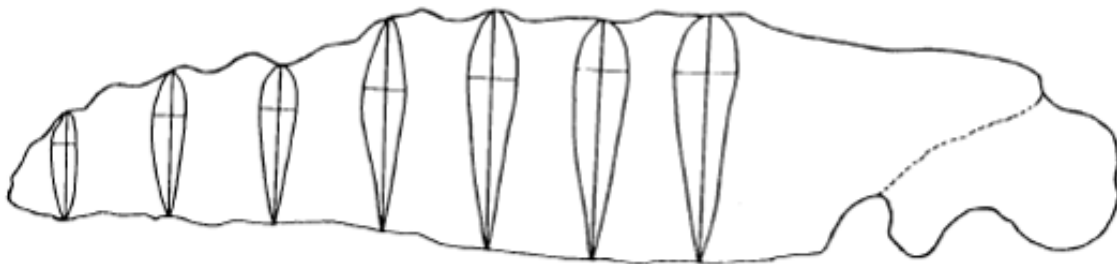


Figure 2: Sketch of a humpback whale pectoral fin [11]

This paper reports the results of a numerical investigation into the effects of a sinusoidal leading edge fitted to NACA0015 and NACA4415 profiles, with the aim of studying the combined effects of a sinusoidal leading edge and camber. The purpose of the research was to provide insight into the physical flow mechanisms associated with a sinusoidal leading edge.

NUMERICAL METHOD

The authors carried out the present analysis using OpenFOAM, an unstructured open-source code intended for the simulation of turbulent flows [16] and based on the finite volume method. They solved the incompressible Navier-Stokes equations with the RANS approach using the Launder-Sharma low-Reynolds number $k-\epsilon$ model [17] and *simpleFOAM* solver. They performed simulations in a steady mode, using a second order QUICK divergence scheme. The authors used a GAMG linear solver for the SIMPLE sub-set and *smoothSolver* for all the other equations with a tolerance set to 10^{-8} for all the computed quantities. They carried out simulations in parallel mode on MATRIX cluster at the CASPUR HPC facility (Rome).

The authors considered two different NACA four-digit profiles, i.e. the NACA0015 symmetric airfoil and the NACA4415 airfoil, respectively, as the un-cambered and the cambered baseline

geometries. They used these profiles to create airfoils with straight leading edge as well as sinusoid leading edge. Table 1 summarises the geometry of the studied test-cases. The sinusoid's amplitude was equal to 2.5% of the chord length to be self-consistent with the open literature. The authors did not study the effect of wavelength as both van Nierop *et al.* [12] and Johari *et al.* [13] studies concluded that the wavelength did not influence the aerofoil performance.

The authors discretised the computational domain, Figure 3, with approximately 2.5 million hexahedral cells in order to keep $y^+ \approx 1.0$ on the airfoil surface. They carried out a grid sensitivity assessment on three two dimensional meshes solving the flow around NACA0015 profile at different AoA. The three meshes comprised approximately 8,000, 30,000 and 60,000 cells respectively. According to the computed lift coefficients, the intermediate mesh was sufficiently dense to achieve grid convergence. Subsequently, the authors extruded the domain in a span-wise direction with 80 cells. They defined the computational domain's extension downstream from the trailing edge, based on experience with previous unsteady RANS computations, to ensure the wake's free flapping. Table 2 illustrates the set of boundary conditions.

Table 1: Details of the investigated cases

Airfoil profiles	NACA0015 and NACA4415
Leading edge lines	Straight and sinusoidal
Mean normalised chord length	$c=1.0$
Sinusoid amplitude of the leading edge	2.5% of c
Wavelength of the sinusoid	$0.25c$
Computational domain	1.3 c upstream of the blade leading edge 9.3 c downstream of the blade trailing edge 0.5 c in spanwise direction (i.e. two sinusoids) 2.0 c in pitchwise directions
Reynolds number	183,000

Table 2: Boundary conditions

Inlet	Steady velocity profile (velocity magnitude =1.0 and different AoA) Turbulence intensity = 1.5% $v_T/v=30$
Outlet	Convective boundary conditions
Blade	No-slip conditions
Pitch- and span-wise directions	Periodicity

To provide a reference solution, the authors computed the airfoils' aerodynamic performance using a quasi three-dimensional viscous analysis based on XFOIL, a public domain program for subsonic isolated airfoils [18].

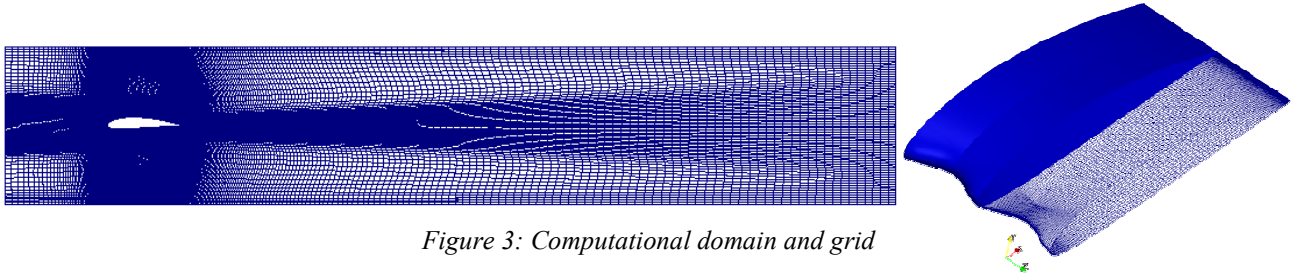


Figure 3: Computational domain and grid

RESULTS

Lift and drag performance

Figure 4 and 5 illustrate the variation of lift and drag coefficients with the AoA. These figures show the results of the three-dimensional simulations plotted against the benchmark XFOIL predictions limited to blades with a straight leading edge. In this case, numerical results provide a good prediction of both coefficients. For the symmetric NACA0015 the discrepancy is almost negligible, while for NACA4415, the authors concluded that the observed 5% discrepancy could be associated with the impact of grid distortion around the blade as well as the virtual blade interaction due to pitchwise periodicity.

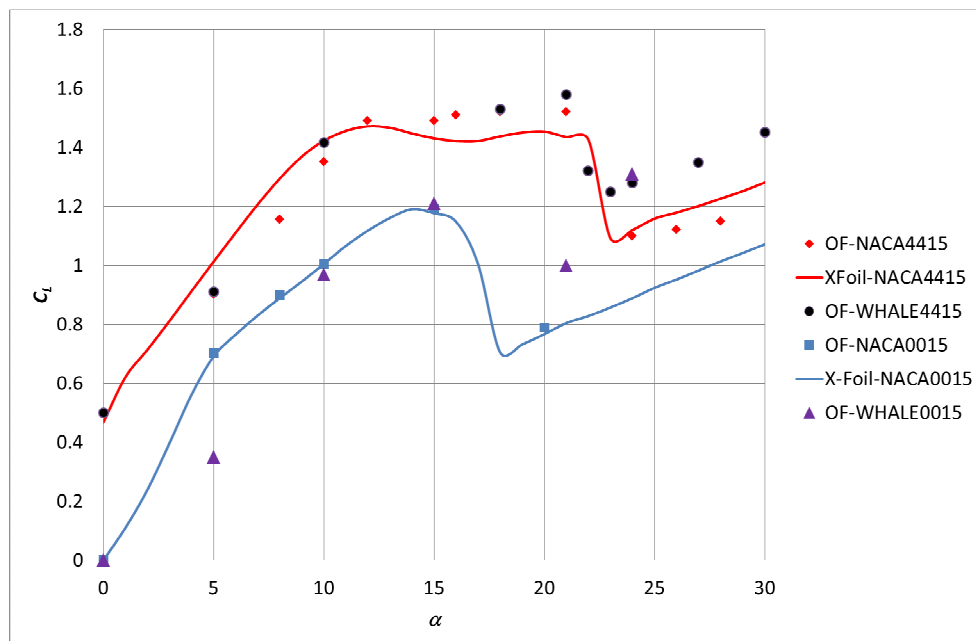


Figure 4: Lift coefficient vs AoA. WHALE0015 and WHALE4415 identify the sinusoidal leading edge blades

The authors used the prediction of both coefficients for the straight leading edge profiles as a reference for the accuracy of the sinusoidal leading edge airfoils (here labelled as WHALE0015 and WHALE4415 following the corresponding NACAxx15 straight leading edge airfoils). Computations for the WHALExx15 airfoils return similarities and discrepancies. In particular, when considering the pre-stall behaviour of WHALE0015, the lift coefficient is lower than the corresponding NACA0015 airfoil. In contrast after stall (that occurs around an AoA of 15 degrees for the NACA profile), the lift coefficient increases significantly. At 21 degrees it is about 20% higher and at 24 degrees the pay-off reaches a peak of 40%. For WHALE0015 the drag coefficient difference with respect to NACA0015 is not significant. This observation is self consistent with the results of Johariet *al.*[13].

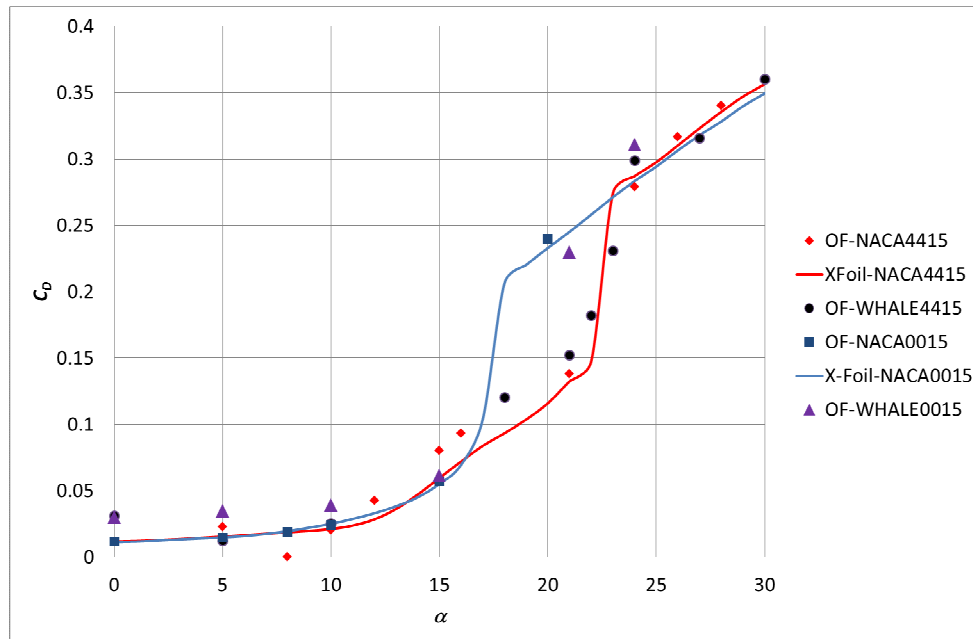


Figure 5: Drag coefficient vs AoA. WHALE0015 and WHALE4415 identify the sinusoidal leading edge blades

Similar figures apply to the aerodynamics of the cambered WHALE4415 airfoil as compared to the straight leading edge geometry. Looking at the pre-stall behaviour, in contrast to the symmetric airfoil pair, the use of leading edge bumps immediately results in a small increase in lift coefficient over the AoA range from $\alpha = 10$ to 20 deg. This small gain in lift is maintained up to the stall incipience, which occurred at 23 degrees. Across and post-stall, the leading edge bumps beneficially influence the lift evolution. First, the airfoil features an early recovery in aerodynamic work capability and then the lift coefficient starts increasing with a steepest slope and a 30% gain.

The evolution of the drag coefficient with the AoA, Figure 5, confirmed the influence of the leading edge geometry over the stall limit. The authors speculate that such an influence results from the control of boundary layer flow separation at the aft of the airfoil. The drag coefficient in the presence of the bumps does not differ from the NACA4415 baseline airfoil, and it appears to reduce in the post-stall range.

Inner workings of leading edge bumps

Table 3 compares the lift-to-drag ratio coefficient at a different AoA. As expected, in view of the analysis of the normalised aerodynamic forces, WHALE0015 airfoil at stall incipience features a significant gain with respect to the straight profile that remains more or less constant after stall. In contrast when compared with the cambered WHALE4415 airfoil, we only find a gain in the post-stall operating region.

We now analyse the effects of the bumps on the velocity and vorticity fields. Figure 6 shows a qualitative view of the recirculation zone at three selected AoAs for WHALE4415 (10 deg, 21 deg and 24 deg). It is evident that separation occurs at the trailing edge at spanwise positions corresponding to the sinusoid's trough; whereas, at spanwise sections corresponding to the sinusoid peak, the flow remain attached even at an AoA of 24 degrees, which is the minimum lift condition after stall. In order to provide further insight into the recirculating region, Figure 7 compares the WHALE4415 streamwise velocity distribution at $x/c = 0.95$ and $Z = 0.5$ and $Z = 1.0$ (leading edge trough and peak) against the same profile for NACA4415.

Table 3: Lift-to-drag coefficient at selected AoA for the airfoils under investigation. (*)

<i>Airfoil</i>	<i>21degrees</i>	<i>24degrees</i>
NACA0015-OF	3.25*	3.20*
WHALE0015-OF	4.35	4.21
NACA4415-OF	11.01	3.94
WHALE4415-OF	10.40	4.29
NACA0015-XFoil	3.28	3.14
NACA4415-XFoil	10.83	3.90

(*)Values are interpolated.

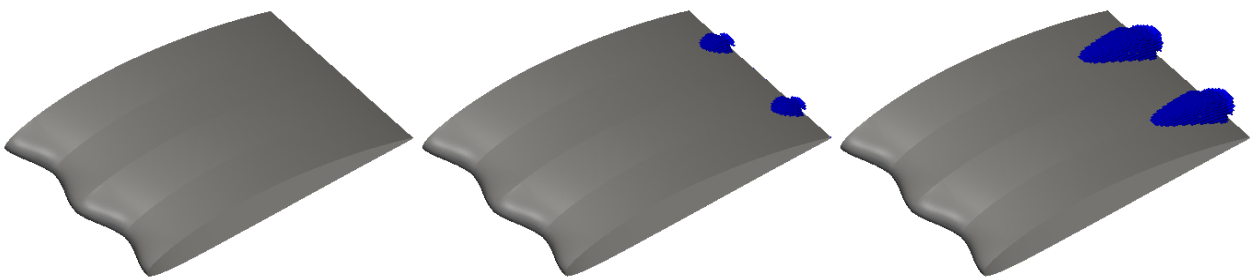


Figure 6: WHALE4415 recirculation zone at various AoA; from left: 10deg, 21deg and 24deg

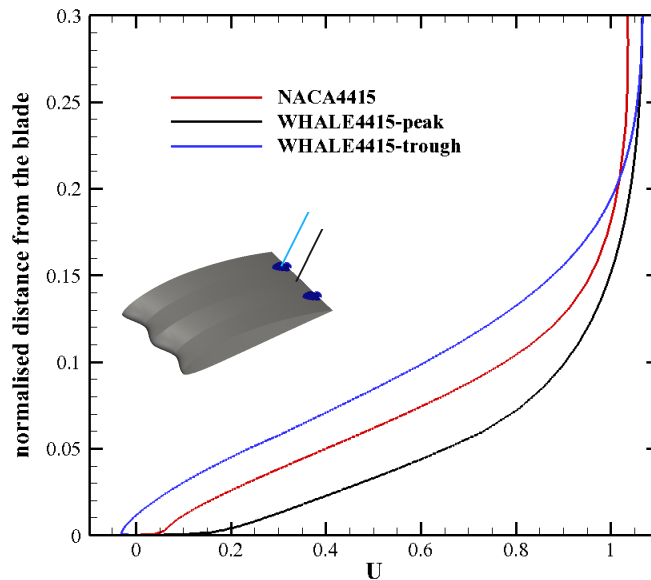


Figure 7: Streamwise velocity profiles at 95% of the blade for $\alpha=21\text{deg}$. NACA4415(red) and WHALE4415 (see sketch)

Figure 8 also presents the effect of the bumps on the velocity field at different distances from the blade suction surface.

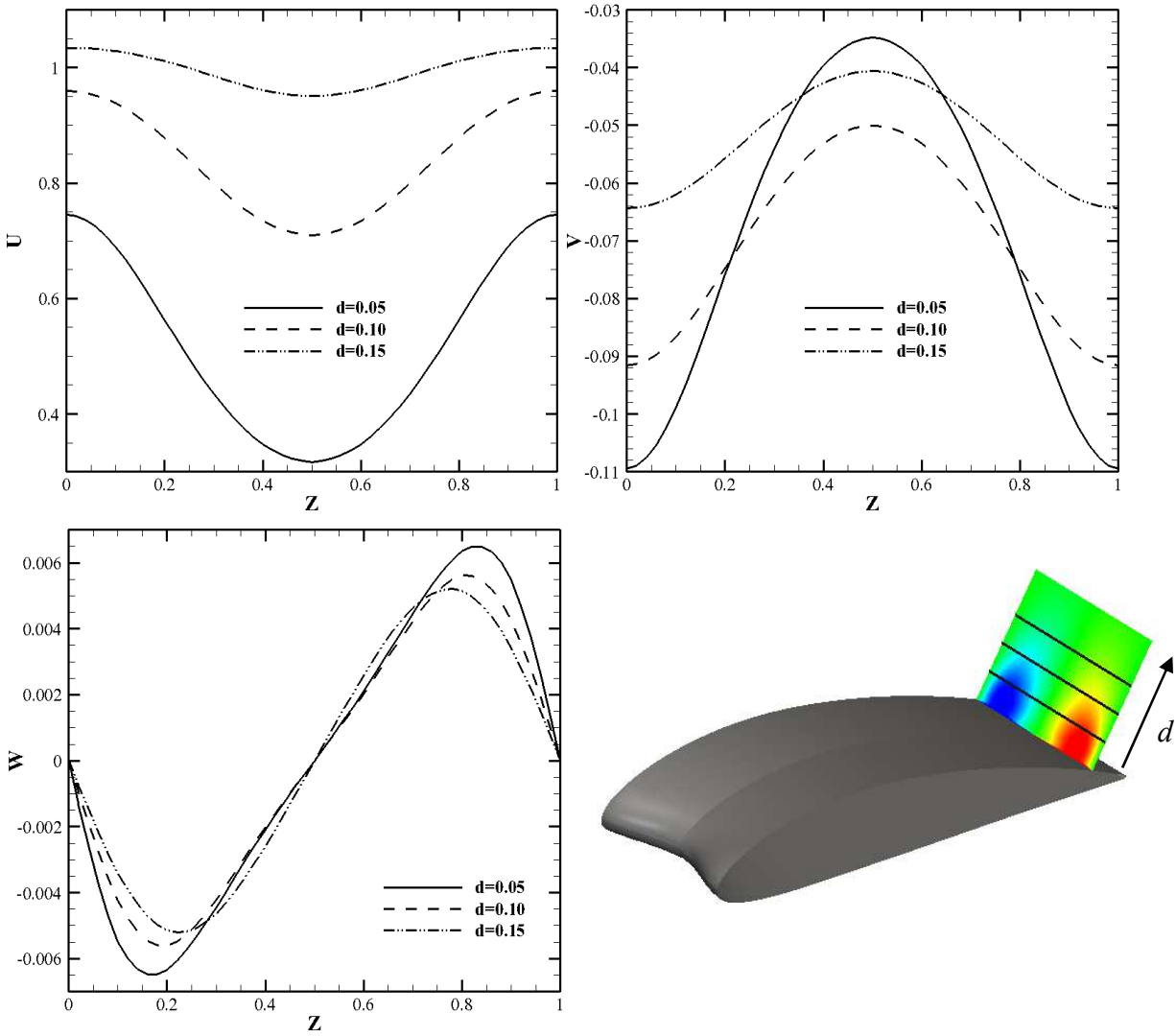


Figure 8: Velocity profiles at 90% of the chord in three different lines at 5%, 10% and 15% of chord distance from the blade surface (see sketch)

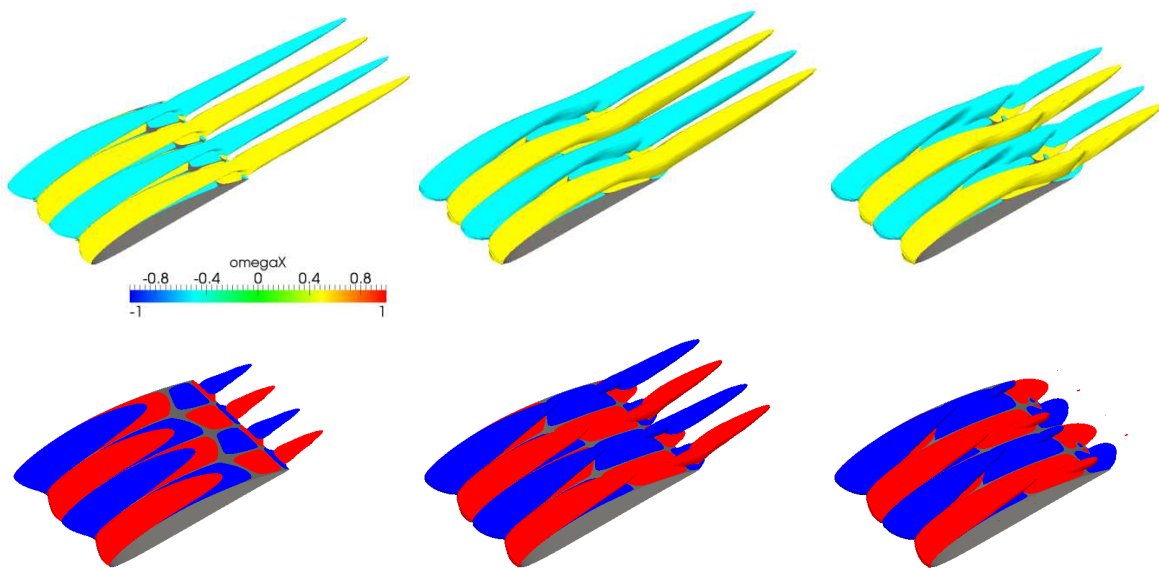


Figure 9: WHALE4415 streamwise component of vorticity iso-surfaces; from left 10deg, 21deg and 24deg; first row $\omega_x = \pm 0.5$; second row $\omega_x = \pm 1.0$

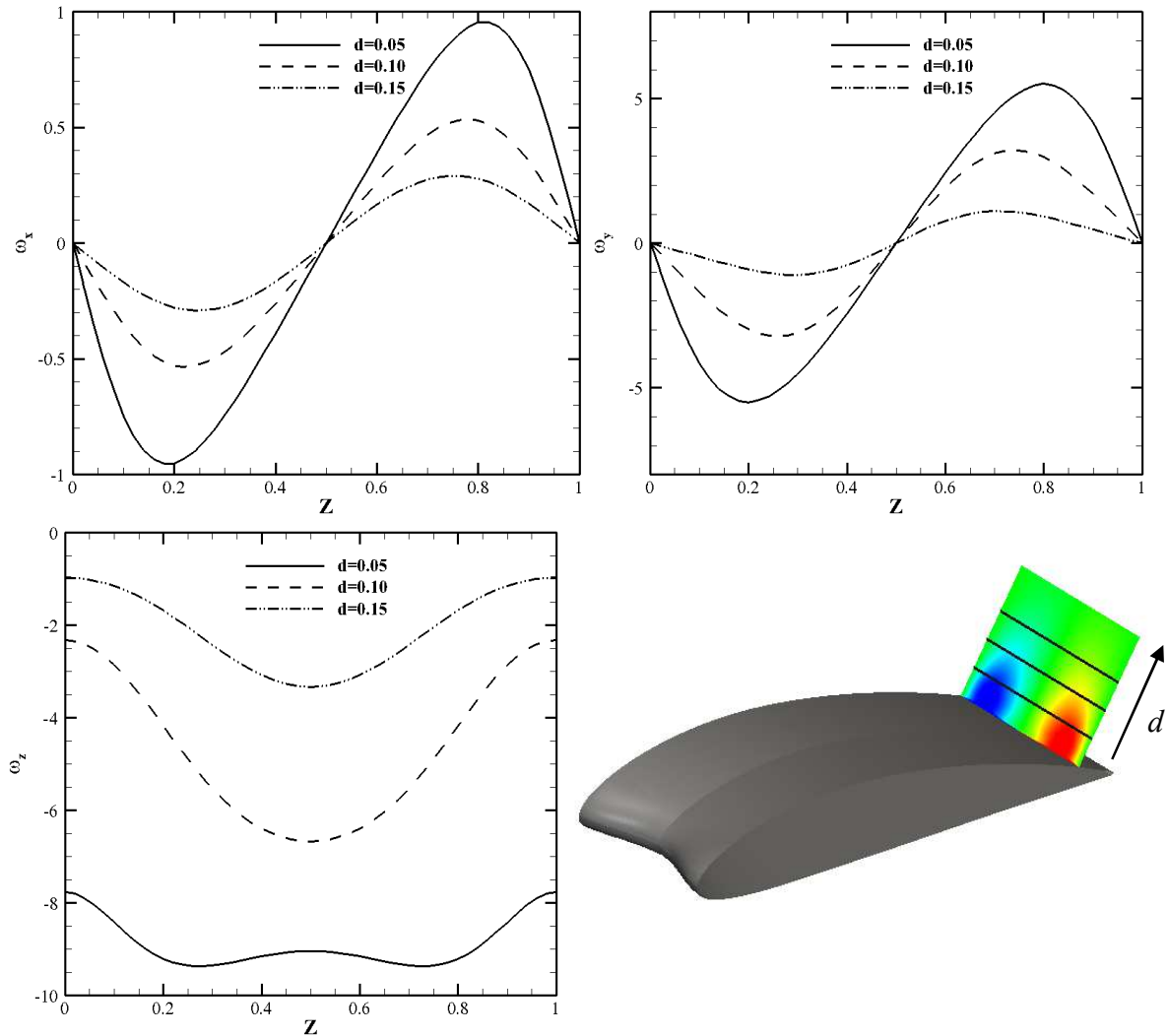


Figure 10: Vorticity profiles at 90% of the chord in three different lines at 5%, 10% and 15% of chord distance from the blade surface (see sketch)

The authors computed all the three components of velocity vector at $x/c=0.90$. The leading edge geometry clearly affects them and results in a sinusoidal pattern in phase with it. The only exception is in the spanwise component that is half a wavelength off-phase as a consequence of the stretch which the bumps induced on the velocity field.

The conspicuous vorticity field, Figure 9, first presents iso-surfaces of a streamwise component at three different AoAs which are pertinent to pre-stall, stall incipience and post-stall. The presence of the bumps generates elongated flow structures, even at an AoA=10 degrees. The re-circulating flow twists these structures when stall occurs at an AoA=21 degrees and appear stretched when the lift is at its minimum, at an AoA=24 degrees.

Figure 10 shows vorticity profiles at different distances from the wall taken at $x/c=0.90$. Apart from the expected attenuation of the vorticity magnitude moving away from the blade, stream and pitchwise components are shifted half a wavelength with respect to the leading edge's sinusoidal shape. The spanwise component, on the contrary, features a more complex behaviour: at distance $d=0.05$, a nearly doubling of the frequency characterises the profile, which is diffused at $d=0.10$. This observation indicates indirect evidence of the non-uniform velocity defect at the WHALE4415 blade's trailing edge.

To give additional insight into the flow topology, Figure 11 presents the enstrophy isosurfaces at pre- and post-stall AoA. At 10 degrees the leading edge geometry deforms the enstrophy field resulting in a mirroring effect as the sinusoid's peak in the leading edge corresponds to the

enstrophy trough at the trailing edge. In contrast at an AoA=24degrees, the enstrophy field reflects the combined effect of both the leading edge geometry and the flow separation regions, resulting in a horseshoe-shaped structure.

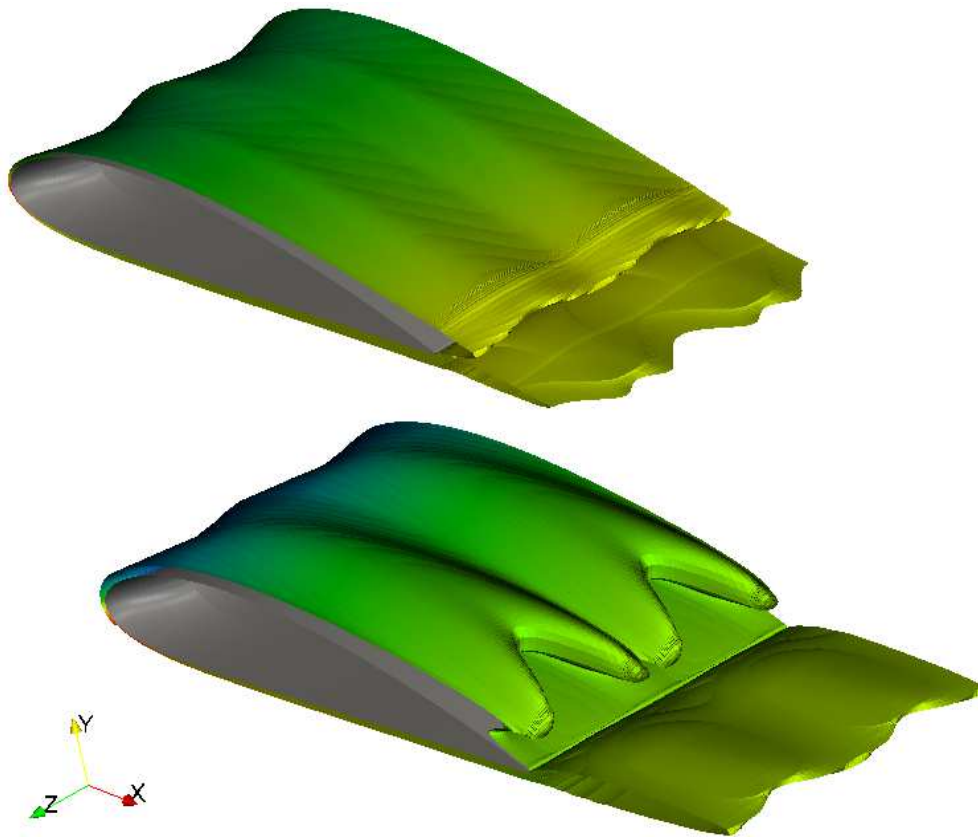


Figure 11: WHALE4415 enstrophy isosurfaces: 10deg (top) and 24deg (bottom) coloured with pressure

CONCLUSIONS

This paper presented a three-dimensional numerical study on the impact of sinusoidal leading edges on cambered airfoil profiles. The study provides insight into the influence of the leading edge geometry at different operating conditions spanning from pre- to post-stall.

The authors carried out the numerical study with OpenFOAM using a RANS $k-\epsilon$ Launder Sharma low-Reynolds closure model.

The authors assessed a modified sinusoidal-shaped leading edge in terms of lift and drag performance. The assessment of the modified geometry on a cambered airfoil entailed the comparison of aerodynamic performance against the same airfoil geometry without a sinusoidal-shaped leading edge, as well as with an un-cambered airfoil.

The evolution of the lift coefficient associated with introduction of a sinusoidal-shaped leading edge modified airfoil performance during stall, with an early recovering in the aerodynamic work capability and a 30% gain in lift after stall for the WHALE4415 airfoil.

The leading edge's geometry directly impacted on the airfoil velocity and vorticity fields. This infers that the stabilising effect on the blade's suction side corresponds to the leading edge sinusoid's peak, as separation on the suction side occurs only at the trailing edge in spanwise cross-sections which correspond to leading edge troughs.

ACKNOWLEDGEMENTS

Fläkt Woods Group and the Dipartimento di Ingegneria Meccanica e Aerospaziale, "Sapienza" University of Rome undertook the present research in the context of the contract FW-DMA09-11. The team carried out computations on MATRIX cluster at the CASPURHPC facility under an STD11-504 grant. The authors want to thank in particular Dr. Michela Botti of CASPUR for her kind support.

NOMENCLATURE

Latin

AoA	angle of attack
c	chord
d	distance from the suction side surface (see inserts in Figure 9 or Figure 10)
C_L	lift coefficient
C_D	drag coefficient
k	turbulent kinetic energy
RANS	Reynolds-averaged Navier Stokes
Re	Reynolds number
U, V, W	stream, pitch and spanwise components of the velocity field
x,y,z	stream, pitch and spanwise directions
Z	normalised spanwise coordinate; $Z = z/\lambda$

Greek

α	angle of attack
ε	stream, pitch and spanwise directions
$\eta = \frac{1}{2} \int_{\Omega} \omega^2 d\Omega$	enstrophy
λ	sinusoid leading edge wavelength
ν_T	turbulent viscosity
ω	vorticity

KEYWORDS

Biomimesis, leading edge bumps, lift control, OpenFOAM.

BIBLIOGRAPHY

- [1]. Gravdahl, J.T. and Egeland, O. (1999), Compressor Surge and Rotating Stall: Modelling and Control. Springer Verlag, London.
- [2]. Langston, L.S. (2009), Fitting a pitch. *ASME Mechanical Engineering Magazine*, vol. 131(12), pp. 38–42.
- [3]. Bianchi, S., Corsini, A., Sheard, A.G. (2011), Stall inception, evolution, and control in a low speed axial fan with variable pitch in motion, accepted for publication in *Journal of Engineering for Gas Turbines and Power*, manuscript reference number GTP-11-1174.
- [4]. Corsini, A. and Rispoli, F. (2004), Using sweep to extend the stall-free operational range in axial fan rotors. *Proceedings of the IMechE, Part A: Journal of Power and Energy*, vol. 218, pp.129–139.

- [5]. Paduano, J.D., Greitzer, E.M., Epstein, A.H. (2001), Compression system stability and active control, *Annual Review of Fluid Mechanics*, vol. 33, pp. 491–517.
- [6]. Liu, Y., Dhingra, M., Prasad, J.V.R., 2009, Active compressor stability management via a stall margin control mode, *ASME Paper No. GT2009-60140*
- [7]. Shyy, W., Lian, Y., Tang, J., Viieru, D. and Liu H., *Aerodynamics of Low Reynolds Number Flyers*. Cambridge University Press, ISBN 978-0-521-88278-1.
- [8]. Fish, F. E. (1993), Influence of hydrodynamic design and propulsive mode on mammalian swimming energetics. *Aust. J. Zool.* Vol 42 pp. 79-101.
- [9]. Fish, F. E., Howle L. E. and Murray M. M. (2008), Hydrodynamic flow control in marine mammals. *Integrative and Comparative Biology*, vol. 48 (6), pp. 788-800.
- [10]. Hua, X., Gu, R., Jin, J., Liu, Y., Ma, Y., Cong, Q., Zheng, Y. (2010), Numerical simulation and aerodynamic performance comparison between seagull aerofoil and NACA 4412 aerofoil under Low-Reynolds. *Advances in Natural Science*, vol. 3(2), pp. 244-250.
- [11]. Fish, F.E. and Battle, J.M. (1995), Hydrodynamic design of the humpback whale flipper. *Journal of Morphology*, vol. 225, pp. 51–60.
- [12]. van Nierop, E.A., Alben, S. and Brenner, M.P. (2008), How bumps on the whale flippers delay stall: an aerodynamic model. *Physical Review Letters*, vol. 100, pp. 054502 (1-4)
- [13]. Johari, H., Henoeh, C., Custodio, D. and Levshin, A. (2007), Effects of leading-edge protuberances on airfoil performance. *AIAA Journal*, vol. 45(11), pp. 2634-2632.
- [14]. Pedro, H.T.C. and Kobayashi, M.H. (2008), Numerical study of stall delay on humpback whale flippers. *46th AIAA Aerospace Sciences Meeting and Exhibit*, Reno, Nevada, USA, 7–10 January.
- [15]. <http://www.whalepower.com>
- [16]. Weller, H.G., Tabor, G., Jasak, H., Fureby, C. (1998), A tensorial approach to continuum mechanics using object-oriented techniques. *Computers in Physics*, vol. 12, pp. 620–631.
- [17]. Launder, B.E. and Sharma, B.R. (1974), Application of the energy-dissipation model of turbulence to the calculation of flow near a spinning disc. *Letters in Heat and Mass Transfer*, vol. 1, pp. 131–138.
- [18]. Drela, M. (1989), XFOil: an analysis and design system for low Reynolds number airfoils. *Conference on Low Reynolds Number Airfoil Aerodynamics*, University of Notre Dame, Indiana, USA.

E-MAIL CONTACTS

Alessandro Corsini: corsini@dma.ing.uniroma1.it

Giovanni Delibra: giovanni.delibra@uniroma1.it

Geoff Sheard: geoff.sheard@flaktwoods.com